Nuclear Engineering and Design 429 (2024) 113616

Contents lists available at ScienceDirect

Nuclear Engineering and Design

journal homepage: www.elsevier.com/locate/nucengdes

Gas permeability and gamma ray shielding properties of concrete for nuclear applications

Daria Jóźwiak-Niedźwiedzka [a,1,*], Marta Choinska Colombel [b,2], Aneta Brachaczek [a,3], Mariusz Dąbrowski [a,4], Jakub Ośko [c,5], Michał Kuć [c,6]

[a] Institute of Fundamental Technological Research, Polish Academy of Sciences, Pawińskiego 5B, 02-106 Warsaw, Poland
[b] Nantes Université, École Centrale Nantes, CNRS, GeM, UMR 6183, F-44600 Saint-Nazaire, France
[c] National Centre for Nuclear Research, ul. A. Sołtana 7, 05-400 Otwock, Poland

ARTICLE INFO

Keywords:
Heavyweight aggregate
Hydrogen-bearing aggregate
Shielding concrete
Gas permeability
Gamma ray attenuation
Microstructure
ITZ

ABSTRACT

Concrete used in nuclear applications faces significant durability challenges due to degradation from radiation, thermal stresses, and chemical reactions. These issues highlight the critical need for impermeable concrete shields to prevent radioactive leaks and protect against harmful radiation. This study examines how concrete composition affects gas permeability and gamma radiation shielding properties. Three coarse aggregates—amphibolite (reference), magnetite, and serpentine—and two cement types (ordinary and slag) were tested, with concrete densities ranging from 2309 to 3538 kg/m^3. Gas permeability was measured using a Cembureau-type constant head permeameter, and gamma shielding was assessed through the linear attenuation coefficient (μ) and half-value layer (HVL) at ^{137}Cs decay energies. The results revealed significant variations in gas permeability and gamma ray shielding based on aggregate and cement type, with observable relationships between gas permeability, HVL, and concrete density. The results obtained from the presented research will contribute to increasing the safety, durability and cost-effectiveness of concrete constructions and maintenance of nuclear facilities.

1. Introduction

With the ongoing need to produce energy and the increasing diversification of its sources while reducing CO_2 emissions, nuclear technology is becoming increasingly important compared to the depleting traditional analysis of energy sources. However, the potential environmental impact and possible crises related to nuclear power are subjects of significant interest and discussion (Y-Ch et al., 2004). Nuclear accidents resulting in radiation leaks have attracted considerable attention from researchers worldwide, as the emissions of gamma rays and neutrons represent the most hazardous types of nuclear and radiation leaks. Additionally, the production of radioactive waste is a major concern due to its high radioactivity, necessitating long-term reliable facilities to protect people in vicinity of the nuclear reactor (Ali et al., 2023).

Therefore, in the construction of buildings with high radiation shielding demands — such as hospitals, research centers, radioactive waste repositories, and nuclear power plants (NPPs) —the properties of the materials used are critically important. Concrete is chosen for these structures not only because of its mechanical strength and long-term durability (Ouda, 2015; Soni et al., 2018; Akkurt et al., 2006) but also due to its effectiveness in attenuating or absorbing radiation (K. William et al., 2013; Jóźwiak-Niedźwiedzka and Lessing, 2019). The cost of shields made from various types of concrete is lower than that of high-density materials such as steel, lead, or depleted uranium, which are used primarily for the direct reactor shielding, (Brandt, 2013).

Gamma rays are attenuated by interactions with electrons, so

* Corresponding author.
E-mail address: djozwiak@ippt.pan.pl (D. Jóźwiak-Niedźwiedzka).
[1] ORCID: 0000-0003-3681-0817.
[2] ORCID: 0000-0003-4799-7226.
[3] ORCID: 0000-0002-8272-4138.
[4] ORCID: 0000-0003-1581-7083.
[5] ORCID: 0000-0001-8966-1507.
[6] ORCID: 0000-0003-2781-0743.

https://doi.org/10.1016/j.nucengdes.2024.113616
Received 29 July 2024; Received in revised form 5 September 2024; Accepted 27 September 2024

concrete used for gamma ray shielding should be designed to maximize its density. The most practical and economically viable shielding against gamma rays can be achieved by using materials with heavy atoms, which are denser than commonly used aggregates (Jóźwiak-Niedźwiedzka and Lessing, 2019). Heavy concrete which is characterized by density above 2600 kg/m^3 is the most commonly used material worldwide for that purpose due to its excellent radiation shielding properties (Jóźwiak-Niedźwiedzka and Lessing, 2019). Mineral ores such as magnetite (Horszczaruk et al., 2015; Horszczaruk and Brzozowski, 2019), barite (Zhou et al., 2023; Zou et al., 2024), limonite (Oto et al., 2015) or siderite (Esen and Doğan, 2017) in the form of aggregates are more popular for producing heavyweight concrete, (Kanagaraj et al., 2023; Aminsharei et al., 2024; Khalaf et al., 2020; Azeez et al., 2019; Akkurt et al., 2012; Shams et al., 2018).

While neutron shielding concrete is designed to manage fast and intermediate neutrons, which need to be slowed down, and thermal neutrons, which must be absorbed or captured. Therefore, it is essential to include materials with atoms capable of both thermalizing and capturing neutrons. The hydrogen atoms in water, chemically bound in concrete, slows down fast neutrons, which could be captured by other atoms, e.g., of boron, known for its large neutron capture cross-section, (Jóźwiak-Niedźwiedzka and Lessing, 2019). Aggregates used in neutron shielding concrete include materials with bound water from hydrated iron ores like serpentine (Zhou et al., 2023; Dąbrowski et al., 2022; Khmurovska et al., 2019), or bauxite (Madej et al., 2024), and aggregates containing boron from natural borate ores like colemanite or ulexite, (Kharita et al., 2011; Lotti et al., 2019; Yadollahi et al., 2016).

Various concrete mixtures have been designed to address specific shielding requirements across a range of nuclear environments. Ultra-high-performance concretes were developed to mitigate electromagnetic interference (Jung et al., 2020), borated paraffin-infused concrete is utilized in boron neutron capture therapy facilities (Pazirandeh et al., 2011), and heavy concrete is tailored for shielding purposes in hospitals offering carbon therapy (Wang, 2023), as well as in radioactive waste storage facilities (Kanagaraj et al., 2023; Elshazli et al., 2023) and has been used in nuclear research centres (Jóźwiak-Niedźwiedzka et al., 2018). While neutron shielding concrete finds application in nuclear power plants (Saklani et al., 2021; Field et al., 2015). However, in NPPs concrete shielding structures vary depending on the reactor cooling methods (Meiswinkel et al., 2013; Bruck et al., 2019). In a pressurized water reactor (PWR), the shielding structure surrounds the reactor and steam generator, including the primary circuit cooling systems, all under one roof, resulting in a large reactor building. In a boiling water reactor (BWR), low-reactivity steam from the primary circuit is directed to the turbine, necessitating a shielding structure within the turbine building to prevent nuclear radiation. In several plant designs, the shielding concrete, also known as the biological shield wall, acts as a load-bearing structure that supports the reactor pressure vessel and other concrete elements above, such as the reactor cavity structure and the operation floor (Bruck et al., 2019). Regardless of the reactor type, the material used in shielding structures at NPPs is designed integrally with other safety systems to prevent the release of radiation or radioactive substances into the environment.

The most critical infrastructure elements concerning NPP safety include are reactor building shielding structures and channels for fuel transportation and radioactive waste storage. To reduce the radiation dose around the reactor building, impermeable concrete shields are constructed also to serve as barriers against harmful radiation. Therefore, the impermeability of concrete shielding structures and their connections with various installations, such as pipe passages for coolant handling potentially contaminated liquids and gases, is a fundamental functional requirement, alongside the necessary shielding against nuclear radiation. This is confirmed by gas permeability test results conducted on second-generation reactors operating in France. After mandatory leak tests, it was found that several reactor containment structures are currently close to the allowable leak limit (Agostini et al., 2015). It was revealed that gas tightness is crucial for reactor safety (Pei et al., 2019). For this reason, various solutions are being sought to improve the tightness of concrete structures.

In nuclear installations, shielding concrete must meet unique requirements associated with radiation (Y-Ch et al., 2004; Kanagaraj et al., 2023), the presence of aggressive chemical substances (Meiswinkel et al., 2013), thermal cycles (Horszczaruk et al., 2015; American Society of Mechanical Engineers, 2007), and mechanical loads (Basu et al., 2013) to provide structural integrity and minimize the risk associated with radiation exposure (Ageing management of concrete structures in nuclear power plants, IAEA Nuclear Energy Series No. NP-T-3.5, International Atomic Energy Agency, Vienna, 2016; Pomaro, 2016). Radiation induces changes in the concrete's microstructure, leading to reduced strength and durability. It is known that compressive strength of concrete decreases with increasing neutron fluence (Pazirandeh et al., 2011; Maruyama et al., 2013) and gamma dose (Sommers, 1969; Soo and Milian, 2001), but the influence of radiation on the potential threat of alkali-silica reaction (ASR) is a new concern, (Jóźwiak-Niedźwiedzka et al., 2018; Maruyama et al., 2017; Tcherner and Aziz, 2009). Another emerging issue is the approach to mechanical loads, such as tsunamis and or earthquakes. After the Fukushima-Daichi accident, it was recognized that extreme natural phenomena should also be considered. Following that catastrophe, the durability of the installation was assessed in the context of Beyond Design Basis Earthquakes (BDBE) (Basu et al., 2013). Increasing levels of seismic activity must also be taken into account. Thus, thermal stresses resulting from thermal cycling can cause thermal cracking and further weaken the structural integrity of concrete. Chemical reactions, such as ASR, can lead to expansive reactions in concrete, resulting in cracking and deteriorations. In addition, mechanical loads caused by unexpected accidents can also worsen the structural integrity of concrete. All these factors significantly affect the permeability of concrete.

Concrete as a typical porous material, has its durability highly dependent on factors such as permeability. It is a critical factor in the longevity and integrity of concrete structures. High permeability can allow the ingress of gases, liquids and harmful chemicals under a pressure gradient, which may degrade concrete matrix and embedded reinforcement.

The vast majority of results regarding gas permeability pertain to ordinary concrete and focus on determining the relationship between pore structure characteristics and the gas permeability of concrete (Chen et al., 2023; Zhang et al., 2018; Das and Kondraivendhan, 2012). The investigation into gas permeability concerning the durability of shielding concrete in nuclear installations is justified, given the specific requirements and challenges associated with this field (IAEA, 2016). Prior studies have provided valuable insights into the impact of shielding concrete composition on gas permeability or radiation shielding capabilities. However, they did not address both issues simultaneously.

In a recent review article on advancements in Portland cement-based radiation shielding concrete (Kanagaraj et al., 2023), the concept of permeability was mentioned only once, specifically in reference to water permeability. Kubissa et al. (Kubissa and Glinicki, 2017) investigated the Autoclam air permeability index (API) of shielding concrete containing CEM I and CEM III cement, as well as heavyweight and hydrogen-bearing aggregates. They revealed that the API index for concrete with addition of barite aggregate was more than 55 % higher than for concrete made with magnetite or serpentinite. The lowest air permeability was achieved by concrete with magnetite aggregate, which was even lower than the reference concrete with amphibolite aggregate. In another study, Kubissa et al. (Kubissa et al., 2018) explored the air permeability of shielding concretes taken from massive blocks and identified a significant difference in API attributed to changes in cement composition. An increase of more than 100 % was observed for ordinary Portland cement (CEM I) compared to blended cement (CEM II). This difference has been linked to a potential connection with microcracks induced by large thermal gradients, especially when the maximum

temperature for drying the specimens was set at 105 °C. However, the results reported by Kubissa et al. (Kubissa and Glinicki, 2017; Kubissa et al., 2018) pertained to a different permeability testing method and did not include results related to shielding properties.

Although the IAEA (IAEA, 2016) recommendations for nuclear containments suggest three methods for determining the air permeability of concrete, namely the Torrent method (R. Torrent et al., 1995), the Autoclam method (Basheer et al., 1995), and the surface airflow method (Whiting and Cady, 1992), these methods primarily focus on testing surface gas permeability. While attempts have been made to dry the surface of concrete samples using various methods (Basheer et al., 2000), they have not produced satisfactory results. Due to the presence of surface moisture gradients (Basheer and Nolan, 2001), the aforementioned methods employ correction factors and graphs to approximate the surface moisture content of concrete, but establishing a consistent relationship is challenging. Therefore, in the research presented in this paper, the Cembureau method was selected, where the lack of moisture content correction is viewed as a positive aspect. Additionally, unlike other methods for determining concrete gas permeability (Beushausen et al., 2019), the Cembureau method offers the advantage of testing the entire concrete sample rather than just the surface layer. The performance criteria are correlated with exposure classes. It is a standardized method (XP P 18-463, 2011) and is used in service life models. Certainly, the Cembureau method is limited to laboratory environments and require specific conditions that are not suitable for real structures. However, the results obtained using the Cembureau technique, under pressure, can serve as a reference, as the gas permeability results obtained with various vacuum methods (like the Torrent Permeameter Tester) show good agreement, regardless of the technique used and even if the tests differ in the type of regime, the duration of the test or the pressure (Sogbossi et al., 2019; Cagnon et al., 2024). While the Cembureau method is standardized (XP P 18-463, 2011) and widely used in construction, it lacks specific adaptations or standard procedures tailored to the unique demands of nuclear applications. This is why we conducted tests on shielding concrete to ensure accurate result interpretation across different nuclear projects. In addition, the Cembureau cell used in this study is associated with a system of thermal mass digital flowmeters (Fabien et al., 2021) which makes it possible to control the nature of the steady-state gas flow directly during the test, thus avoiding any measurements artefacts.

Several studies have been carried out to improve the shielding properties of concrete against ionizing radiation (Y-Ch et al., 2004; Jóźwiak-Niedźwiedzka and Lessing, 2019; Aminsharei et al., 2024; Pazirandeh et al., 2011; Wang, 2023). Previous research has provided valuable insights into the interplay between concrete composition (Horszczaruk and Brzozowski, 2019; Masoud et al., 2023; Lardhi and Mukhtar, 2023), its durability (Horszczaruk and Brzozowski, 2019; Dąbrowski et al., 2022), and gamma radiation shielding capabilities (Zhou et al., 2023; Khalaf et al., 2020; Azeez et al., 2019; Amin et al., 2023). It has been shown that the radiation shielding properties of concrete are paramount in structures where protection against gamma radiation is imperative.

This article delves into the key considerations and findings related to the air permeability and shielding properties of concrete in structures with high radiation shielding requirements. In high radiation shielding applications, it's important to minimize gas permeability in order to maintain the integrity and effectiveness of the gamma ray shielding. Concrete with low gas permeability helps to prevent the ingress of air, moisture, or other contaminants that could compromise the shielding properties over time. Hence, research was conducted on shielding concrete containing special aggregates, such as magnetite and serpentinite, concerning its permeability and gamma ray shielding capacities. Microstructure investigations were carried out, and correlations between the analysed properties of shielding concrete were determined. The obtained results contributed to the development of improved standards and guidelines for concrete used in nuclear applications, supporting ongoing efforts to enhance safety and environmental protection in the nuclear industry.

2. Experimental programe

2.1. Materials

Two types of cement were used in the research, ordinary Portland cement CEM I 42,5 R and blended cement containing ground granulated blast furnace slag CEM III/A 42,5N-HSR/NA, referred in the article as CEM I and CEM III. Siliceous sand ($\rho = 2.65$ kg/m^3) was used as the fine aggregate. Three different coarse aggregates were used: reference amphibolite aggregates, and special aggregates used in shielding concrete: magnetite and serpentinite aggregates. Serpentinite aggregate is characterized by an increased water content of 12.1 %. The mineral composition determined by the XRD method (Fig. 1), indicated that the magnetite aggregate contained, as expected, magnetite itself and magnesioferrite. Primarily antigorite and, to a lesser extent, lizardite were the dominant serpentine polymorphs. Both antigorite and lizardite are common serpentine minerals, and their presence in serpentinite is typical. Amphibolite was primarily composed of amphibole minerals and plagioclase with minor amounts of quartz and biotite were also found. The chemical admixture consisted of a high-range water reducer (HRWR) based on modified polycarboxylates. Detailed chemical composition of the cements and aggregates and their loss on ignition are presented in Table 1. Physical properties are shown in Tables 2 and 3.

2.2. Mix proportion and preparation of specimens

The absolute volume method described in ACI standard practice (Aci, 2002) was utilized to optimize the arrangement of selected special aggregates. This method was tailored to meet local conditions, with the volume-based packing of aggregate grains was specified by (PN-B-06265:, 2018). To ensure conformity with standard curves (PN-B-06265:, 2018) and achieve an optimal aggregate gradation, siliceous river sand comprised 20 % of the volume fraction in concrete incorporating magnetite and serpentinite aggregates. In contrast, for reference concrete made with amphibolite, 30 % of the volume was dedicated to siliceous sand to obtain a similar aggregate gradation. The gradation of aggregate mixtures is shown in Fig. 2.

Eight concrete mixtures were designed as illustrated in Table 4: four incorporating CEM I and four utilizing CEM III. Amphibolite aggregates of 2–8 mm and 8–16 mm fractions, accompanied by river sand of 0–2 mm, were used in the reference concretes (CEM I – A1 and CEM III – A3). Concretes were fabricated incorporating solely magnetite (M1 and M3) and serpentinite aggregates (S1 and S3), as well as those containing a combination of the aforementioned aggregates (MS1 and MS3). The labels 1 and 3 correspond to cement types CEM I and CEM III, respectively. Magnetite aggregates of 0–5 mm and 0–16 mm fractions, along with serpentinite aggregates of 0–2, 2–8, and 8–16 mm fractions, were used. The concrete containing both special aggregates included magnetite in the 0–5 mm fraction and serpentinite in the 2–8 and 8–16 mm fractions. The amount of sand in the concretes containing special aggregates was correspondingly lower compared to the reference concrete due to the presence of fine fractions of magnetite (0–5 mm) and serpentinite (0–2 mm) with w/c = 0.48. The admixture was added to ensure a similar consistency of the mixtures.

During the mixing process, initially coarse and fine aggregates were mixed for 3 min in the mixer. Subsequently, cement was introduced into the mixture along with water and HRWR, and the mixing process was continued for 5 min.

Two cylindrical specimens (100x200 mm) and three cubic specimens (150 mm) were prepared from a one batch for each mixture. These specimens were cast in PVC moulds and compacted using a mechanical vibrator. Subsequently, the specimens were subjected to moist curing at 20 ± 1 °C and 90 ± 5 % relative humidity for 28 days.

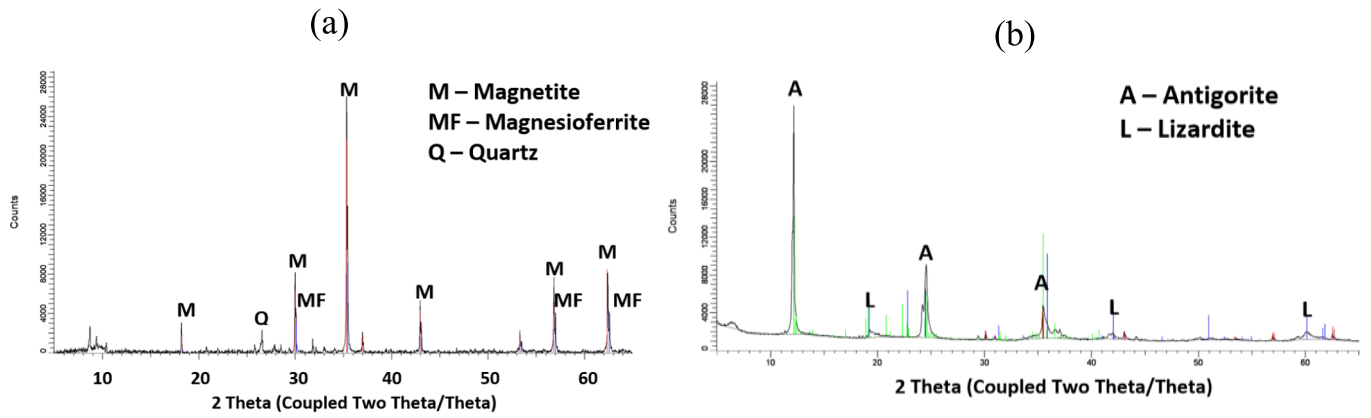

Fig. 1. XRD patterns with main characteristic peaks in the tested special aggregates: (a) magnetite, (b) serpentinite.

Table 1
Chemical composition of cements and coarse aggregates measured by XRF method (% wt) and loss on ignition (LOI).

Constituent	Cement		Coarse aggregate		
	CEM I	CEM III	Amphibolite	Magnetite	Serpentinite
SiO_2	19.69	30.30	45.48	2.19	38.51
Al_2O_3	4.82	6.25	11.40	0.51	0.73
Fe_2O_3	3.28	1.54	12.07	91.72	7.99
CaO	61.19	51.84	11.20	0.72	0.54
MgO	2.94	4.55	10.49	0.84	38.97
SO_3	3.19	3.07	0.01	0.00	0.06
Na_2O	0.22	0.44	2.08	0.19	0.11
K_2O	0.95	0.63	0.83	0.10	0.00
TiO_2	0.25	0.28	2.02	0.34	0.00
Mn_2O_3	0.09	0.12	0.27	0.11	0.12
SrO	0.06	0.07	0.01	0.00	0.00
ZnO	0.01	0.02	0.01	0.00	0.01
P_2O_5	0.13	0.16	0.00	0.85	0.00
LOI	3.10	0.74	2.58	2.42	12.96

Table 2
Density and physical properties of cements used in the research (data from the cement producer).

Properties	CEM I	CEM III
Density, kg/m^3	3.11	3.01
Initial setting time, min	223	256
Final setting time, min	302	327
f_{c2}, MPa	29.40	16.70
f_{c28}, MPa	54.70	54.40
Le Chatelier soundness, mm	0.33	0.44
Specific surface area (Blaine), cm^2/g	3973	4757

Table 3
Density, physical and mechanical properties of aggregates.

Properties	Amphibolite	Magnetite	Serpentinite
Density, kg/m^3	2.90	4.80	2.60
Water absorption[1], %	0.7	0.2	1.1
Freeze-thaw resistance[2], %	0.5	0.2	2.3
Aggregate crushing value[3], %	–	11.2	5.6

[1] PN-EN 1097–6:2013 (PN-EN, 2013);
[2] PN-EN 1367–1:2007 (PN-EN, 2007);
[3] PN-B-06714–40: 1978 (PN-B-06714-40:, 1978).

Following the 28-day curing period, the density of the cubic specimens was determined based on their measured dimensions and weight. Compressive strength tests were carried out on three cubic specimens for each material composition at the end of the 28-day period. For gas permeability testing, one cylindrical specimen was used, also at 28 days. To measure gas permeability, a concrete cylindrical specimen was cut with a diamond saw, obtaining three specimens of 50 mm thick discs. These discs were then dried at 80 °C until a constant mass was achieved (appr. two weeks). Another cylindrical specimen was designated for microstructural analysis and to determine the gamma-ray attenuation parameters after 28 days. This specimen was sliced using a diamond saw to obtain cross-sections with a thickness of about 9 mm.

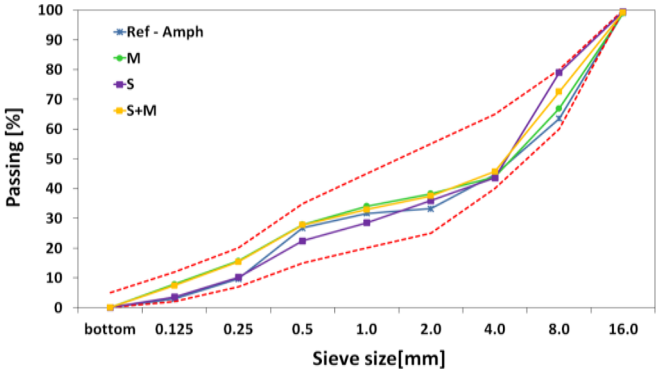

Fig. 2. Gradation curve of aggregates by volume (dashed red lines indicate limits of optimal particle packing according to (PN-B-06265:, 2018). (For interpretation of the references to colour in this figure legend, the reader is referred to the web version of this article.)

2.3. Methods

After 28 days of curing, the density of cubic specimens with a volume of 150 mm^3 was determined based on their measured dimensions and weight, according to PN-EN 12390–7 (PN-EN 12390, 2020). The compressive strength of concrete was determined on the three specimens 150 mm^3 after 28 days of curing in accordance with the PN-EN 12390–3:2019 (PN-EN 12390–3, 2020) using 2000 kN Controls® testing machine, applying a constant loading rate of 500 N/s.

Gas permeability tests were conducted on cylindrical specimens with a diameter of 100 mm and a height of 50 mm. Before testing, after 28 days of curing in water, the specimens were dried at a temp. of 80 °C to a constant mass. Temperature was chosen for two reasons. First, such gentle conditioning ensures the even distribution of moisture in the concrete without deterioration of the cement matrix. Higher temperatures may cause microcracks, significantly affecting the results (Choinska et al., 2007) and 80 °C is the critical temperature at which shielding concrete can function (American Society of Mechanical Engineers, 2007; IAEA, 2016). The specimens were then cooled during 48 h

Table 4
Concrete constituents in kg/m$^{3.}$

Mix ingredients	CEM I				CEM III			
	A1	M1	S1	MS1	A3	M3	S3	MS3
CEM I	350	350	350	342	0	0	0	0
CEM III	0	0	0	0	350	350	350	342
Sand 0–2 mm	593	371	371	362	593	371	371	362
Amphibolite 2–8 mm	628	0	0	0	628	0	0	0
Amphibolite 8–16 mm	750	0	0	0	750	0	0	0
Magnetite 0–5 mm	0	839	0	879	0	839	0	879
Magnetite 0–16 mm	0	1846	0	0	0	1846	0	0
Serpentinite 0–2 mm	0	0	273	0	0	0	273	0
Serpentinite 2–8 mm	0	0	909	477	0	0	909	477
Serpentinite 8–16 mm	0	0	273	477	0	0	273	477
Water	168	168	168	164	168	168	168	164
HRWR, % m.c.	0.43	0.64	3.00	1.97	0.36	0.57	1.71	1.24

in a desiccator at 20 ± 1°C before measurement was started. The intrinsic gas permeability results were obtained using Klinkenberg regression (Klinkenberg, 1941) on the apparent permeability, measured using four different inlet pressures. The gas permeability results, corresponding to the intrinsic values, are averages of three specimens.

Initial and second rates of water absorption were tested according to ASTM C1585 (ASTM C1585-20, 2020). Similar to the gas permeability tests, three cylindrical specimens (100 mm in diameter and 50 mm in height) for each type of concrete were dried at a temp. of 80 °C to a constant mass before testing. This procedure was consistent with the findings of Castro et al. (Castro et al., 2011), who stated that it is not recommended to condition specimens at 105 °C because it may adversely affect the microstructure of the specimens. The specimens were subsequently wrapped with plastic waterproof sheets, thoroughly sealed on their sides and bottom, with only the top surface remaining uncovered. The uncovered surface of the specimen was positioned face down on a support structure (plastic rods) within a container filled with water, maintaining a level 3 ± 1 mm above the top of the device. The mass of the specimens was recorded at regular intervals – more frequently during the first 6 h, and less frequently thereafter – over a period of 8 days. The initial rate of water absorption, known as initial sorptivity (S_1) was calculated based on mass gained during the first 6 h, while secondary sorptivity (S_2) was determined from the mass gained between 24 h to 8 days of exposure.

The concrete microstructure evaluation was performed on polished specimens using a scanning electron microscope with micro-areas analysis (SEM-EDS). Specimen preparation involved cutting them to dimensions of 25x40x10 mm, followed by a 3-day drying period at temperature 50 °C and impregnation with epoxy resin. Next, the specimens were ground on diamond discs with grit sizes of 125, 75, 54, 18, and 9 μm, and polishing with diamond pastes with grit sizes of 6, 3, 1, and 0.25 μm. Then, the specimens were dried again for 3 days at temp. 50 °C before applying a carbon coating approx. 20 nm thickness to enhance imaging. Microstructural examination was conducted using a JEOL JSM-6460LV scanning electron microscope (SEM), complemented by an energy-dispersive X-ray spectroscopy (EDS) detector (PV72-55050 EDAX, AMETEK, USA, running Genesis Spectrum 6.2 software by EDAX Inc.). This fallowed for both qualitative (element identification) and quantitative (elemental concentration) analyses of the specimens' constituents. The SEM-EDS operated with an acceleration voltage of 20 kV, an aperture of 110 μm, and a working distance of 8–9 mm.

To evaluate the gamma-ray shielding parameters and attenuation factor for various concretes, a test stand was prepared in accordance with the EN 61331–1 standard (EN 61331-1, 2014) (refer to Fig. 3). Tests were conducted in a certified calibration laboratory (accreditation No. AP 070 issued by the Polish Centre for Accreditation). Drawing from prior studies on radiation shielding of concrete specimens (Domanski et al., 2016), measurements were executed using a Tema Sinergie IM6M automatic irradiator equipped with a ^{137}Cs gamma-ray reference source and a F1 type tissue equivalent parallel plate recombination ionization chamber developed and constructed by National Centre for Nuclear Research (Golnik et al., 2014). The chamber has 3.8 cm^3 active volume, 34 mm electrodes diameter and is filled with ethane up to 0.5 MPa. The distance between electrodes is equal to 1.75 mm. For the applications presented in the publication, the detector operated at a saturation voltage of 1000 V.

The active centre of the detector was positioned at a distance of 85 cm from the source, where the air kerma rate was measured to be$\dot{K}_{air}$ =

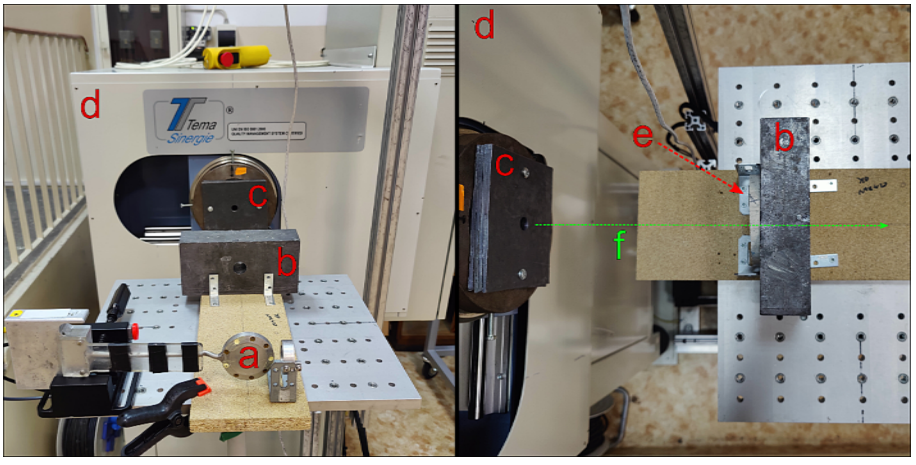

Fig. 3. View of the test stand, a – F1 type recombination chamber, b, c – lead collimators, d – Tema Sinergie IM6M automatic irradiator, e – specimen, f – ^{137}Cs radiation beam direction.

28.0 ± 1.4 mGy/h. During the measurements each concrete specimen was positioned between two lead collimators so that the gamma radiation beam and the detector were arranged in specimen axis. The tests were carried on for 4 cover layer thicknesses from 9 mm to 41 mm, adding subsequent specimen slices and separately one test for 50 mm thick specimen from another batch. For each specimen thickness, 40 measurements of the ionization current were performed using a new algorithm based on fast measurements in a charge mode (Kuć, 2023; Kuć et al., 2024).

The results of dosimetric measurements were used to calculate the attenuation factor (k) values for all concrete samples, from which the linear attenuation coefficient (μ) and Half-Value Layer (HVL) were determined. The attenuation factor (k) is defined as the ratio of the ionization current measured by an ionization chamber without a shield (i_0) to the ionization current measured behind a shield of thickness d ($i_s(d)$):

$$k(d) = \frac{i_0}{i_s(d)} \tag{1}$$

and μ is the parameter of the k(d) exponential curve:

$$k(d) = e^{\mu d} \tag{2}$$

Taking into the expanded uncertainty of the attenuation factor was approximated as 2 % for each measurement (calculated using exact differential method). HVL and μ were calculated for each specimen. HVL, is the thickness of a material required to reduce the air kerma of an X-ray or gamma ray to half its original value.

The linear attenuation coefficient is a constant that describes the fraction of attenuated incident photons in a monoenergetic beam per unit thickness of a material (Huda and Slone, 2003).

Because of the linear relationship $\ln \frac{i_0}{i_s}$ (d), μ can be determined as the slope of the line and uncertainty u_μ is standard error of the estimation using least squares method:

$$ln \frac{i_0}{i_s(d)} = \mu d \tag{3}$$

The Half-Value Layer (HVL) was calculated according to the equation:

$$HVL = \frac{\ln(2)}{\mu} \tag{4}$$

The uncertainty of HVL was determined from the uncertainty of u_μ, according to the relationship:

$$u_{HVL} = HVL \bullet \frac{u_\mu}{\mu} \tag{5}$$

3. Results

The change in cement type from CEM I to CEM III had no significant impact on the volume of HRWR dosed, as measured by the slump cone method at the assumed consistency, Table 5. However, increasing the proportion of fine fractions of serpentinite resulted in a higher dosage of HRWR. In all concretes from both the CEM I and CEM III series, the intended consistency was achieved without exceeding the maximum dosage of admixture specified in the technical data sheet.

Density and compressive strength values determined after 28 days of curing are presented in Table 5. The reference concretes A1 achieved a density of 2495 kg/m^3 and A3 = 2486 kg/m^3. As expected, concretes with magnetite aggregate exhibited the highest density, measuring 3583 kg/m^3 with CEM I and 3499 kg/m^3 with CEM III. The lowest density was characteristic of concretes with serpentinite aggregate, approximately 2319 ± 10 kg/m^3.

Concretes made with Portland cement CEM I exhibited compressive strengths ranging from 57 to 70 MPa, whereas concretes with slag cement CEM III showed strengths of 61 to 73 MPa. The reference concrete with amphibolite aggregate, regardless of the type of cement used, demonstrated a compressive strength of approximately 59 ± 2 MPa. The highest compressive strength was exhibited by concrete with magnetite aggregate, achieving 70 MPa with CEM I and 73 MPa with CEM III. A decrease in compressive strength is observed when using serpentinite aggregate compared to magnetite aggregate. For ordinary Portland cement CEM I, the decrease is 17 %, while for slag cement CEM III, the decrease is 15 %.

Gas permeability and rate of water absorption results are presented in Table 6. Concretes made with slag cement CEM III showed reduced gas permeability compared to those made with ordinary Portland cement CEM I. Among all concretes, those with serpentinite aggregate exhibited the highest gas permeability, while those with magnetite aggregate showed the lowest for both types of cement. Concretes containing serpentinite aggregate demonstrated higher gas permeability, approximately 74 % and 119 % more than concretes with magnetite aggregate, for ordinary Portland cement and slag cement, respectively. Concretes with both magnetite and serpentinite aggregates showed average gas permeability. The initial rate of water absorption was highest in concretes with serpentinite aggregate and lowest in those with magnetite, regardless of cement type. However, cement type also influenced the results, with concretes containing CEM I showing a higher initial rate of water absorption compared to those with slag cement.

The SEM-EDS analysis yielded detailed insights into the microstructure of the cement matrix, elemental composition, and distribution within the coarse aggregate, as depicted in Figs. 4-6. Both fine and coarse aggregates were evenly dispersed in the examined concrete specimens. However, variations were observed in the interfacial transition zone (ITZ) between the coarse aggregate and cement matrix. For concrete made with magnetite aggregate, a dense layer was distinctly visible, contrasting with the discontinuity zones observed with serpentinite aggregate. These zones measured approximately 40 ± 13 μm wide in concrete with CEM I and about 29 ± 11 μm wide in concrete with CEM III (Fig. 5), showcasing the influence of cement type on the width of this layer. Notably, a denser cement matrix-aggregate contact zone was

Table 5
Values of the slump of the fresh mix and density and compressive strength, determined after 28 days of concrete maturity.

Properties		CEM I				CEM III			
		A1	M1	S1	MS1	A3	M3	S3	MS3
Slump	mm	120	120	90	150	120	130	140	140
Density	kg/m^3	2495	3538	2329	2723	2486	3499	2309	2712
	SD	30	42	25	24	34	30	35	39
Compressive strength	MPa	57	70	58	67	61	73	62	69
	SD	1.4	1.6	1.3	1.9	0.9	1.7	1.6	1.1

SD – standard deviation

Table 6
Gas permeability and rate of water absorption values.

Properties		CEM I				CEM III			
		A1	M1	S1	MS1	A3	M3	S3	MS3
Gas permeability (10^{-17})	m^2	2.50	1.48	2.58	2.20	2.00	0.96	2.10	1.80
	SD	0.29	0.27	0.36	0.30	0.23	0.26	0.32	0.31
Initial rate of water absorption S_1 (10^{-2})	$mm/s^{-1/2}$	1.31	1.12	1.35	1.20	1.20	0.96	1.28	1.13
	SD	0.08	0.07	0.07	0.05	0.04	0.04	0.08	0.05
Second rate of water absorption S_2 (10^{-2})	$mm/s^{-1/2}$	0.024	0.021	0.057	0.031	0.022	0.020	0.049	0.027
	SD	0.001	0.001	0.003	0.002	0.001	0.001	0.002	0.001

SD – standard deviation

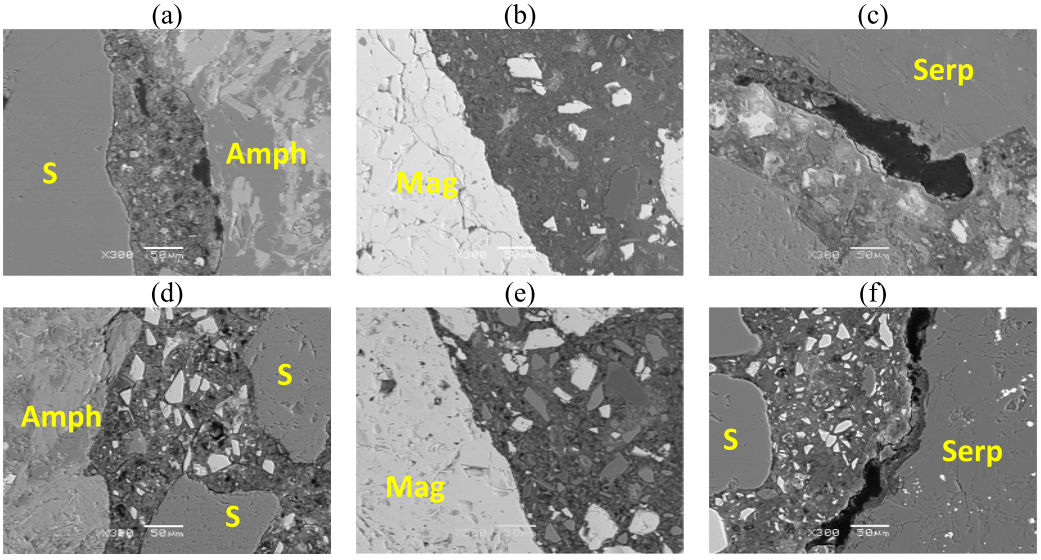

Fig. 4. SEM-BES image showing the interfacial transition zone between cement matrix and coarse aggregate: (a-c) CEM I, (d-f) CEM III; amphibolite Amph, magnetite Mag, serpentinite Serp, sand S.

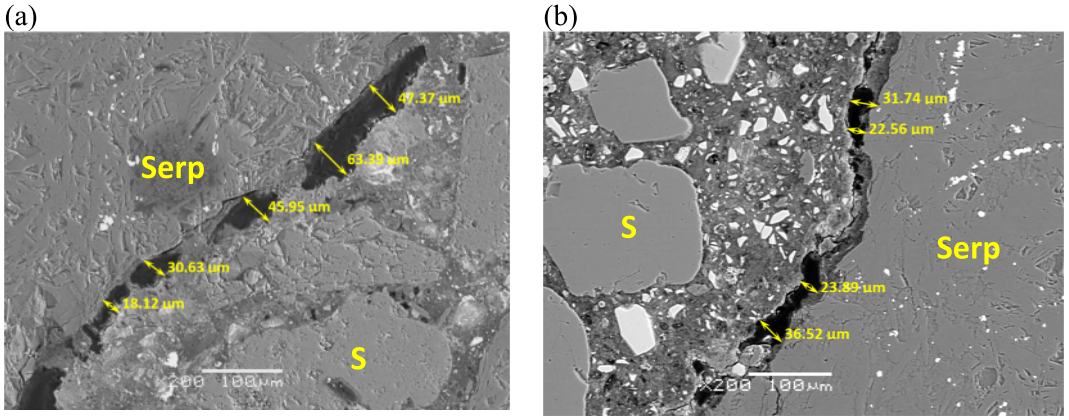

Fig. 5. SEM-BES image showing the differences in the width of the interfacial transition zone between cement matrix and serpentinite aggregate: (a) S1 ~ 40.1 µm, (b) S3 ~ 28.5 µm; serpentinite Serp, sand S.

observed with slag cement (Fig. 5). In the concrete made with amphibolite aggregate, singular discontinuities between the matrix and aggregate grains were evident in CEM I concrete, whereas for CEM III the ITZ zone appeared dense and compact. Moreover, in concrete containing ordinary Portland cement, a layer of portlandite approximately 23.6 ± 3 µm thick surrounded the serpentinite aggregate grains. This layer caused a shift of discontinuities between the aggregate grains and cement matrix towards the cement matrix (Fig. 6).

Table 7 presents the gamma-ray attenuation parameters for the eight concretes, including the attenuation factor (k), linear attenuation coefficient (µ), and half-value layer (HVL). The highest attenuation factor was found in concrete with magnetite aggregate, followed by concretes containing magnetite and serpentinite aggregate, as well as amphibolite and serpentinite. Concretes M1 and MS1 showed attenuation factors

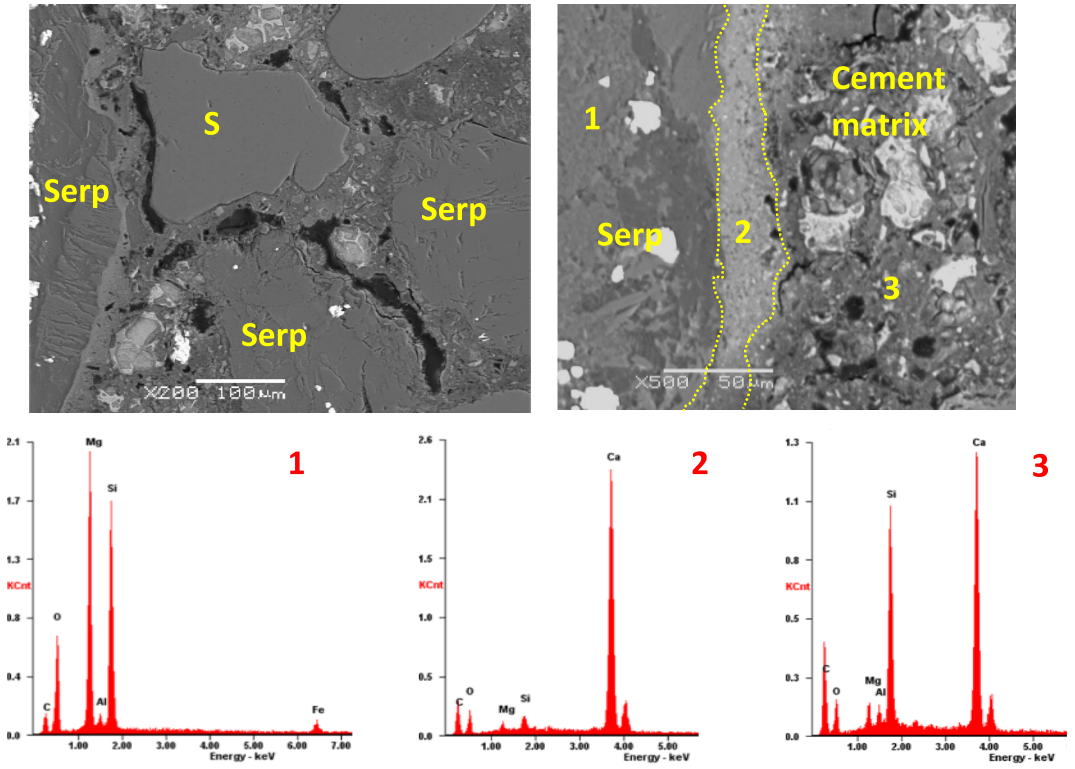

Fig. 6. SEM-BES image showing the layer of portlandite, discontinuities, and air pores in concrete with ordinary Portland cement and serpentinite aggregate: serpentinite Serp, sand S.

Table 7
The results of the attenuation of ^{137}Cs gamma radiation for analysed concretes.

Properties		CEM I				CEM III			
		A1	M1	S1	MS1	A3	M3	S3	MS3
Attenuation factor, k		2.61	4.30	2.47	2.91	2.67	3.85	2.44	2.74
	SD	0.05	0.09	0.05	0.06	0.05	0.08	0.05	0.05
Linear atten. coef. μ	cm^{-1}	0.195	0.294	0.181	0.217	0.197	0.277	0.179	0.208
	SD	0.001	0.002	0.001	0.002	0.001	0.004	0.001	0.003
Half-value layer, HVL	cm	3.56	2.34	3.82	3.13	3.50	2.44	3.84	3.24
	SD	0.01	0.01	0.01	0.03	0.01	0.03	0.01	0.05

SD-standard deviation

respectively 10.5 % and 5.7 % higher compared to concrete with slag cement. The influence of cement type on the reference concrete with amphibolite and serpentinite aggregate was considered negligible. Regarding HVL, the lowest values were characteristic of concretes with magnetite aggregate, while the highest values were found in concrete with serpentinite aggregate.

4. Disscussion

In concrete incorporating serpentinite aggregate, particularly in the fine fractions, higher quantities of high-range water reducer were required, as anticipated based after available literature, (Dąbrowski et al., 2022; Kuć et al., 2024; Sayyadi et al., 2022; Lehner and Gołaszewski, 2021). Awadeen et al. (Awadeen et al., 2024) examined ultra-high-performance heavyweight concretes incorporating special aggregates such as serpentinite, barite, and hematite, and similarly found that mixes with serpentinite exhibited the lowest slump. The decrease in slump was explained by Sayyadi et al. (Sayyadi et al., 2022), who attributed it to the water absorption of serpentinite aggregates and their rough surface, which decreased the workability of concrete.

As expected, concretes with magnetite aggregate exhibited the highest density (~3500 kg/m^3), followed by those with both magnetite and serpentinite aggregates (~2700 kg/m^3). Slightly higher density values were obtained for concretes with magnetite aggregate and ordinary Portland CEM I compared to concretes with slag cement CEM III. However, for the remaining concretes, the influence of cement type on density was negligible. Although Sayyadi et al. (Kuć et al., 2024) demonstrated that replacing a part of the gravel aggregate with serpentinite increased concrete density; however, the serpentinite aggregate studied had a density of 2.7 g/cm^3, whereas in this research, it was 2.6 g/cm^3. Conversely, Lehner and Gołaszewski (Lehner and Gołaszewski, 2021) showed that among the investigated special concretes, those containing serpentinite aggregate (0–16 mm) exhibited the lowest density (2275 ± 17 kg/m^3) and the density of hardened serpentinite concrete tested by Ouda (Ouda, 2015) was 2520 kg/m^3. A similar value of the density (2650 kg/m^3) of hardened concrete with serpentinite aggregate and 2300 kg/m^3 for concrete containing chrysotile aggregate was obtained by Zayed et al. (Zayed et al., 2021; Zayed et al., 2024).

The small fraction of serpentinite aggregate led to a reduction in concrete compressive strength by approximately 15 % compared to concrete containing magnetite aggregate, though, it remained similar to reference concretes with amphibolite aggregate. Azzez et al. (Azeez et al., 2019) achieved similar density values up to 3563 kg/m^3 but significantly lower compressive strength (26–45 MPa) for heavy concrete, despite a lower w/c of 0.4. However, this was attributed to the use of various high-density coarse aggregates, including steel slag, steel shot, iron ore, and limestone aggregate. In contrast, Kubissa et al. (Kubissa et al., 2018) and Dąbrowski et al. (Dąbrowski et al., 2022) achieved comparable compressive strength results. Jain et al. (A. Jain et al., 2023) also confirmed that the use of serpentinite in concrete decreased its strength. Additionally, Sayyadi et al. (Sayyadi et al., 2022) observed a decrease in compressive strength with an increase in serpentinite aggregate content in concrete. With a serpentinite aggregate content exceeding 25 %, the compressive strength of concrete decreased. According to the authors (Sayyadi et al., 2022), this was due to weak hydration of the cement paste and insufficient adhesion between the cement paste and the serpentinite aggregates in the concrete. Conversely, Dąbrowski et al. (Dąbrowski et al., 2022) explained the decrease in compressive strength in concrete with serpentinite by the increased porosity in the contact zone between the serpentinite aggregate and the cement matrix. Abdullah et al. (Abdullah et al., 2022) noted weakness at the ITZ in serpentinite concrete, as the coarse aggregates had a highwater absorption rate, resulting in internal bleeding at the aggregate surface and formation of a porous ITZ. However, according to Awadeen et al. (Awadeen et al., 2024), it was concluded that the use of different special aggregates, including serpentinite, did not affect the hydration reaction based on SEM observations showing similar crystalline structures on the surfaces of specimens. Nonetheless, clear differences are evident in the microstructure of concretes containing serpentinite aggregate, as observed in the conducted research. This variance in observations likely arises from the type of specimens analysed. Awadeen et al. (Awadeen et al., 2024) conducted SEM analysis on fracture surfaces, while in this case, the microstructure was examined on polished specimen surfaces. The ITZ between the aggregate and cement matrix is believed to be approx. 25 – 70 μm thick and is characterized by high porosity and a large amount of hydrated crystalline products such as portlandite and ettringite (Yang et al., 1998). Studies based on SEM analysis indicate that the thickness of ITZ ranges from 10 to 50 μm (Chen et al., 2024), but they did not concern concrete with special aggregate. In the conducted microstructural analysis, it was found that the ITZ between the serpentinite aggregate and the cement matrix was highly porous, measuring approximately 40 μm in concretes S1 and about 28 μm in S3 concrete. Simultaneously, the presence of portlandite layers was observed on some grains of serpentinite aggregate. This finding is consistent with earlier research by Dąbrowski et al. (Dąbrowski et al., 2022), who revealed that the width of the contact zone of increased porosity around the serpentinite grains was approx. 40 to 60 μm. The increased porosity of the ITZ in serpentinite-containing concrete is directly linked to a 15 % reduction in compressive strength compared to concrete with magnetite aggregate, which has a denser ITZ. This higher porosity weakens the cement-aggregate bond, leading to lower strength. The presence of portlandite layers further weakens the ITZ, particularly in CEM I concretes, while slag cement results in a more compact, less porous ITZ. This is partly due to the significantly higher water absorption of serpentinite aggregate compared to magnetite (Table 3). Chen et al. (Chen et al., 2024) confirmed that aggregate water absorption plays a crucial role in ITZ microstructure formation, while observations by He et al. (He et al., 2020) revealed that ITZ weakness stems from microcracks, excessive porosity, and a high concentration of portlandite crystals. Shi et al. (Shi et al., 2020) noted that while the effect of ITZ on concrete permeability is not fully understood, they provided a formula to predict apparent permeability by considering the multi-scale pore structure and ITZ. The observed microstructural features concerning shielding concrete are consistent with literature data (Awadeen et al., 2024). The rough surfaces of heavy-weight aggregates exhibit a strong connection between the aggregates and the paste. This enhancement in ITZ bonding is likely to increase the strength, elastic modulus, and radiation shielding resistance of heavyweight radiation shielding concrete mixes (Awadeen et al., 2024). Similar results were reported by Zayed et al. (Zayed et al., 2021), who investigated shielding concretes containing barite and chrysotile, a variety of serpentine, and found a superior ITZ layer in concrete with barite. The barite grains were highly interlocked with the cement paste, resulting in a very small or almost non-existent ITZ, whereas a porous layer was clearly visible between the serpentine grains and the cement matrix.

Durability is also affected: serpentinite aggregate concrete exhibits gas permeability values approximately 74 % and 119 % higher than those of magnetite aggregate concrete for CEM I and CEM III, respectively. Concrete with serpentinite aggregate exhibited the highest values of gas permeability and initial rate of water absorption, while those with magnetite aggregate showed the lowest. Additionally, all concretes made with slag cement showed reduced both gas permeability and initial rate of water absorption compared to those made with ordinary Portland cement. The above results are supported by the literature data (Sayyadi et al., 2022; Tracz, 2016; Hager et al., 2019). Tracz (Tracz, 2016) showed lower gas permeability in slag cement pastes compared to ordinary Portland cement pastes and revealed that the C-S-H phase in pastes made with CEM III was more compacted and less porous than in the ordinary cement pastes. Hager et al. (Hager et al., 2019) found that concretes with CEM III showed lower permeability and higher compressive strength for both basalt and gravel aggregates concretes compared to CEM I concretes. Whereas Sayyadi et al. (Sayyadi et al., 2022) demonstrated that while replacing 25 % of sand with serpentinite aggregate reduces water absorption, the use of coarse fraction serpentinite aggregates increased water absorption in all tested concretes. The highest water absorption was observed in the concrete containing 100 % serpentinite aggregate. Jain et al. (A. Jain et al., 2023) in review paper also described similar findings regarding serpentinite aggregate. The relationship between initial sorptivity, gas permeability, and compressive strength of concrete was found (Fig. 7). It shows that higher compressive strength correlates with lower initial sorptivity and gas permeability. Greater compressive strength results, as well as lower gas permeability in slag cement-based concretes compared to ordinary Portland cement-based concretes, were due to a denser and less porous cement matrix and interfacial transition zone. It was partially confirmed by Fabien et al. (Fabien et al., 2021). They reported that increased aggregate size in concretes made with CEM I and CEM III resulted in decreased mechanical strength and increased gas permeability. However, Jaya et al. (Jaya et al., 2011) demonstrated that the connection between the compressive strength of concrete and permeability coefficient was notably affected by curing times and was sensitive to the fineness of cementitious materials. Abbas's view (Abbas et al., 2000) can

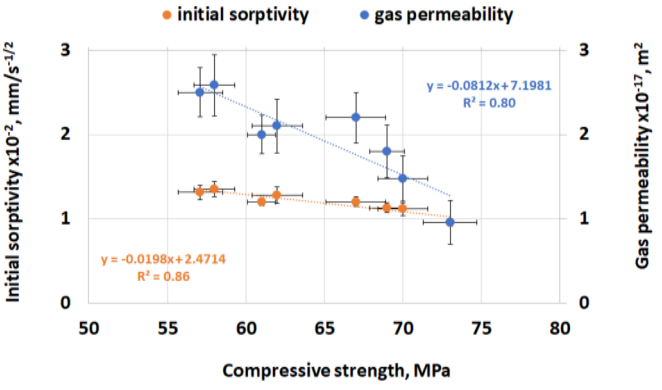

Fig. 7. Relationship between initial sorptivity and gas permeability of concrete vs compressive strength.

be considered here, which states that the relationship between gas permeability and compressive strength can be more accurately interpreted as a trend rather than a single, definitive relationship.

The attenuation factor for the same thicknesses of the specimens was used to quantify the reduction in ionization current caused by the presence of various concrete shields. It is a crucial parameter in radiation detection, as it assesses how shielding materials attenuate radiation, (Shams et al., 2018). Fig. 8 shows the relationship between compressive strength and k vs density of concrete. It shows a clear trend where higher density correlates with increased compressive strength and attenuation factor. Al-Humaiqani et al. (Al-Humaiqani et al., 2013) analysed heavy concrete containing barite and hematite and revealed that as the strength increased, the attenuation of γ-rays also increased. Additionally, just like in conducted research, it was demonstrated that the compressive strength and attenuation of γ-rays have a nearly linear relationship. Saafan et al. (Saafan et al., 2023) arrived at similar conclusions using magnetite aggregate and steel particles. The obtained gamma attenuation results confirm that material composition is a critical factor in optimizing concrete's shielding capabilities (Alkarrani, 2024). Similar to the use of iron additions (ALMisned et al., 2024), borosilicate glass (ALMisned et al., 2024), WO_3/PbO (Zakaly, 2023), or WO_3 and Bi_2O_3 micro and nanoparticles (Tekin et al., 2018) in concrete shields. Other materials, such as polymer-based (Abualroos et al., 2023; Tekin et al., 2020; Alkarrani, 2024) or polymer-lead composites (Ihsani et al., 2024) have also been studied. It has been found that appropriately modifying tiny particles that have high atomic numbers within the epoxy matrix enhances the radiation shielding efficiency of these materials, making them suitable for gamma radiation shielding applications. However, unlike shielding concrete, these materials cannot be used as construction materials due to their low mechanical properties and also an ionizing radiation can alter the structure and properties of polymers (Ihsani et al., 2024).

Fig. 9 illustrates the relationship between gas permeability and half-value layer (HVL) versus the concrete density. It is evident that there is an almost perfect match between the values of HVL and the density of concrete, as expected (Ouda, 2015; Jóźwiak-Niedźwiedzka and Lessing, 2019; Azeez et al., 2019; Klinkenberg, 1941; Mostofinejad et al., 2012; Esfahani et al., 2021). Additionally, the relationship between gas permeability and concrete density was found. In the literature, results regarding the relationship between gas permeability and porosity (Tracz, 2016; Hager et al., 2019; Zhang et al., 2022), relative humidity (Kubissa and Glinicki, 2017), or mechanical properties (Hager et al., 2019; Miah et al., 2019) can be found. However, there is a lack of information concerning the correlation of gas permeability and density of heavy concrete. While Kubissa et al. (Kubissa and Glinicki, 2017) presented air permeability index as a function of concrete density index, they did not establish any dependency. Only the relationships between density and permeability have been studied for soil (Miana Radja et al., 2021).

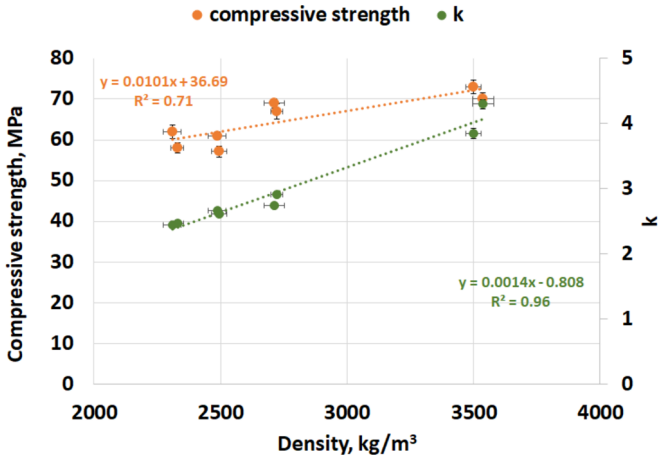

Fig. 8. Relationship between compressive strength and attenuation factor k vs density.

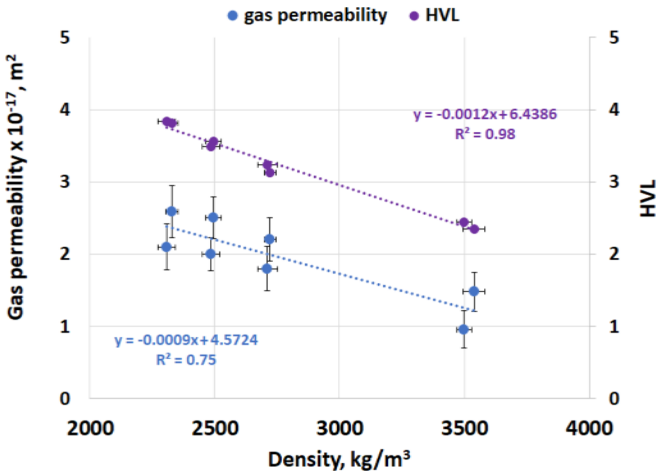

Fig. 9. Relationship between gas permeability and HVL values vs concrete density.

The results obtained from study of Mostofinejad et al. (Mostofinejad et al., 2012) showed that the attenuation of γ-rays in concrete was directly related to the density of concrete. Therefore, it was found that each internal factor increasing the density of concrete will correspondingly increase the value of the radiation attenuation coefficient of the concrete. However, not all density-improving agents simultaneously enhance gas tightness. Despite the improvement in gamma shielding properties of the bentonite clay mixture by adding steel slag, the authors (Isfahani et al., 2019) obtained a more permeable material for water and gas penetration.

Regarding the effect of long-term exposure to gamma radiation on the gas permeability of shielding concrete, it is known that over time, this type of radiation can cause microstructural changes in concrete, including the disintegration of chemical bonds in the cement matrix (Field et al., 2015; Pomaro, 2016). A dose of 100–200 MGy corresponds to the exposure of concrete used as a biological shield during 80 years of power plant operation (Němeček et al., 2023). Cement paste shrinks due to the radiolysis process under the influence of gamma radiation and the evaporation of pore water due to radiation heat (Pomaro, 2016), which promotes the formation of microcracks in the cement matrix. However, gamma radiation on the order of several MGy caused microstructural effects, such as changes in carbonate speciation, which correlated with a decrease in volumetric porosity (Reches, 2019). At the same time, the mass, dimensions, and mechanical properties of concrete did not deteriorate significantly (Reches, 2019). It was also shown that the carbonation depth was linearly dependent on gamma radiation at a maximum dose of 1.6 MGy, which resulted in a reduction of concrete porosity (Jóźwiak-Niedźwiedzka et al., 2022). Depending on the gamma radiation dose, microstructural changes can affect the porosity of concrete, potentially leading to changes in the gas permeability of concrete. The degree of change in gas permeability depends on factors such as the type of radiation, its intensity, duration of exposure, and the specific composition of the concrete.

Concrete with high radiation shielding requirements should possess low gas permeability and effective shielding properties against gamma radiation. Achieving these characteristics involves careful material selection, mix design optimization, and quality control throughout the production process. The obtained results suggest that the type of cement, aggregate, and the proportion of aggregate fractions significantly affect the dosage of HRWR, consistency, density, and compressive strength of the concrete. Additionally, there's a noticeable difference in

compressive strength when comparing concretes made with different aggregates, especially when using special aggregates like serpentinite. The type of cement and aggregate used in concrete production significantly influences both gas permeability and the initial rate of water absorption. Slag cement generally leads to reduced gas permeability compared to ordinary Portland cement. Serpentinite aggregate tends to increase gas permeability and initial water absorption rates, while magnetite aggregate tends to reduce them. The SEM-EDS analysis revealed differences in the microstructure and ITZ characteristics based on the type of cement used and the type of coarse aggregate. These findings provide valuable insights into the interfacial properties and potential durability and shielding efficiency of the special concrete.

Comprehensive assessment of the developed concrete shielding mixtures necessitates additional research. Besides examining the discussed transport properties and associated microstructural aspects, the material's durability in a nuclear setting will be influenced by prolonged exposure to radiation. Research will be carried out to evaluate this impact. Additionally, investigations will be conducted to measure the gas permeability of the shielding concrete using a range of techniques, including non-destructive methods. Another area for future research concerns the effects of mechanical and/or thermal loading on the development of microcracking (in relation with ITZ) and changes in the shielding properties of the studied concretes.

5. Conclusions

This research uniquely explores the effects of varying aggregate types (amphibolite, magnetite, and serpentine) and cement types (ordinary and slag) on both gas permeability and gamma radiation shielding. While concrete performance in nuclear structures has been studied before, the combination of these specific variables and their dual impact on permeability and radiation shielding is relatively novel.

Based on the conducted research, the following conclusions may be formulated:

- There is a noticeable difference in density and compressive strength when comparing concretes made with different aggregates, especially when using special aggregates like serpentinite. Concrete with serpentinite aggregate was characterized by the lowest density and the lowest compressive strength, justified on the microstructural scale by the presence of defects and discontinuities at the interfacial transition zone.
- The type of cement and aggregate significantly influence both gas permeability and the rate of water absorption in concrete. Slag cement generally reduces gas permeability and water absorption rate compared to ordinary Portland cement. Serpentinite aggregate tends to increase gas permeability and initial water absorption rates, while magnetite aggregate tends to decrease them.
- The gamma-ray attenuation properties of concrete are influenced by the type of aggregate and cement used. Concrete with magnetite aggregate tends to exhibit higher attenuation factors. Additionally, the choice of cement type can also impact gamma-ray attenuation, with ordinary Portland cement generally providing higher attenuation compared to slag cement.
- Concrete with magnetite aggregate is characterized by the lowest gas permeability and the highest shielding properties against gamma radiation among the analysed concretes.
- The development of a porous zone around serpentinite aggregates significantly influenced the compressive strength, gas permeability, and radiation shielding properties of the concrete.
- The relationship between gas permeability, the Half-Value Layer (HVL), and the density of concrete has been found and may be used to evaluate in a simplified way shielding performances of concrete, without resorting to a complex radiation test.

A quantitative relationship between compressive strength, gas permeability, initial water absorption, and radiation attenuation, which offering practical insights for optimizing concrete mix designs for specific performance criteria were presented.

The obtained results may lead to design more effective impermeable concrete shields, reducing the risk of radioactive leaks and enhancing protection against harmful radiation. This directly contributes to the safety and efficiency of nuclear facilities. The advantages result of this work lie in its potential to enhance safety, durability, and cost-effectiveness in nuclear facility construction and maintenance. In addition, using slag cement instead of Portland cement for shielding concrete can significantly reduce the carbon footprint and contribute to a more favorable environmental impact. Although aggregates such as magnetite or serpentinite are mined and can lead to resource depletion, the durability of concrete made from these materials plays a crucial role in their overall lifecycle. More durable concrete reduces the need for frequent replacements and repairs, which in turn decreases the demand for new materials and the associated environmental impacts.

CRediT authorship contribution statement

Daria Jóźwiak-Niedźwiedzka: Writing – review & editing, Writing – original draft, Supervision, Methodology, Investigation, Funding acquisition, Formal analysis, Data curation, Conceptualization. **Marta Choinska Colombel:** Writing – review & editing, Writing – original draft, Supervision, Investigation. **Aneta Brachaczek:** Writing – review & editing, Methodology, Investigation. **Mariusz Dąbrowski:** Writing – review & editing, Resources, Methodology, Investigation. **Jakub Ośko:** Writing – review & editing, Methodology, Investigation. **Michał Kuć:** Writing – review & editing, Methodology, Investigation.

Declaration of competing interest

The authors declare that they have no known competing financial interests or personal relationships that could have appeared to influence the work reported in this paper.

Data availability

No data was used for the research described in the article.

Acknowledgment and Funding sources:*

Acknowledgment to the French Embassy in Poland for the Séjour Scientifique de Haut Niveau French Government Scholarship in 2023 for a research trip for Daria Jóźwiak-Niedźwiedzka.

References

A. Jain, V. Agrawal, R. Gupta, Using serpentine in concrete: A literature review, Materials Today: Proceedings, doi: 10.1016/j.matpr.2023.03.138.

Abbas, A., Carcasses, M., Ollivier, J.P., 2000. The importance of gas permeability in addition to the compressive strength of concrete. Mag. Concrete Res. 52 (1), 1–6. https://doi.org/10.1680/macr.2000.52.1.1.

Abdullah, M.A.H., Rashid, R.S.M., Amran, M., Hejazii, F., Azreen, N.M., Fediuk, R., Voo, Y.L., Vatin, N.I., Idris, M.I., 2022. Recent trends in advanced radiation shielding concrete for construction of facilities: materials and properties. Polymers 14, 2830. https://doi.org/10.3390/polym14142830.

Abualroos, N.J., Yaacob, K.A., Zainon, R., 2023. Radiation attenuation effectiveness of polymer-based radiation shielding materials for gamma radiation. Radiat. Phys. Chem. 212, 111070. https://doi.org/10.1016/j.radphyschem.2023.111070.

Aci, 2002. 211.1-91, Standard Practice for Selecting Proportions for Normal, Heavyweight, and Mass Concrete. Am. Concrete Inst.

Ageing management of concrete structures in nuclear power plants, IAEA Nuclear Energy Series No. NP-T-3.5, International Atomic Energy Agency, Vienna, 2016, pp. 372.

Ageing Management of Concrete Structures in Nuclear Power Plants, International Atomic Energy Agency IAEA, Nuclear Energy Series, NP-T-3.5, (2016) pp. 372.

Agostini, F., Skoczylas, F., Masson, B., 2015. Sealing of Concrete Confining Structures of French Nuclear Reactors 28–30, 343–352.

Akkurt, I., Basyigit, C., Kilincarslan, S., Mavi, B., Akkurt, A., 2006. Radiation shielding of concretes containing different aggregates. Cem. Concr. Compos. 28 (2), 153–157. https://doi.org/10.1016/j.cemconcomp.2005.09.006.

İ. Akkurt, C. Başyiğit, A. Akkaş, Ş. Kılınçarslab, B. Mavi, K. Günoğlu, Determination of some heavyweight aggregate half value layer thickness used for radiation shielding. 121 (2012) Acta Physica Polonica A, No. 1, Proceedings of the International Congress on Advances in Applied Physics and Materials Science, Antalya 2011, 138-140.

Al-Humaiqani, M.M., Shuraim, A.B., Hussain, R.R., 2013. Effect of compressive strength on γ-radiation attenuation coefficients for high performance concrete. Int. J. Eng. Sci. Technol. 5 (5), 566–572. https://doi.org/10.7763/IJET.2013.V5.619.

Ali, M.A.E.M., Tawfic, A.F., Abdelgawad, M.A., Wagih, M., Omar, A., 2023. Potential uses of different sustainable concrete mixtures in gamma and neutrons shielding purposes. Prog. Nuclear Energy 157, 104598. https://doi.org/10.1016/j.pnucene.2023.104598.

H. Alkarrani, G. ALMisned, H.O. Tekin, A benchmarking analysis on different rubber materials: towards customisation of lightweight and effective radiation protection solutions for aerospace and electronic applications. J Rubber Res (2024). doi: 10.1007/s42464-024-00272-4.

H. Alkarrani, G. ALMisned, H.O. Tekin, Assessing the efficacy of some heavy-metal infused concrete mixtures in gamma-ray and neutron shielding applications, Radiat. Phys. Chem, 223 (2024) 111988, doi: 10.1016/j.radphyschem.2024.111988.

American Society of Mechanical Engineers, 2007. Boiler and Pressure Vessel Code Section III -Rules for Construction of Nuclear Facility Components Division 2 - Code for Concrete Containments. ASME.

Amin, M., Elemam, W.E., Kandil, M.A., Samy, M., 2023. Effect of heavy-weight recycled materials on radiation shielding and properties of high-strength concrete with CEM III. J. Build. Eng. 79, 107819. https://doi.org/10.1016/j.jobe.2023.107819.

Aminsharei, M.H., Nikbin, I.M., Parvini Sani, H., 2024. Radiation shielding properties of heavy-weight concrete and heavy-weight geopolymer concrete incorporating nano-ZnS. Nucl. Eng. Des. 424, 113240. https://doi.org/10.1016/j.nucengdes.2024.113240.

ASTM C1585-20, Standard test method for measurement of rate of absorption of water by hydraulic-cement concretes, ASTM International, 1-6, 09/01/2020.

Awadeen, M., Amin, M., Bakr, R.H., Tahwia, A.M., 2024. Mechanical properties, attenuation coefficient, and microstructure of ultrahigh-performance heavyweight concrete for radiation shielding applications. J. Build. Eng. 82, 108395. https://doi.org/10.1016/j.jobe.2023.108395.

Azeez, M.O., Ahmad, S., Al-Dulaijan, S.U., Maslehuddin, M., Naqvi, A.A., 2019. Radiation shielding performance of heavy-weight concrete mixtures. Constr. Build. Mater 224, 284–291. https://doi.org/10.1016/j.conbuildmat.2019.07.077.

B.K. Soni, Rajnikant Makwana, S. Mukherjee, N. L. Singh, K. Katovsky, Different concrete compositions as a reactor shielding material for neutrons and gamma rays, Proceedings of the DAE Symp. on Nucl. Phys. 63 (2018), 1080-1081.

Basheer, P.A.M., Montgomery, F.R., Long, A.E., 1995. Clam" tests for measuring in-situ permeation properties of concrete. Non-Destructive Testing and Evaluation 12 (1), 53–73. https://doi.org/10.1080/10589759508952835.

Basheer, P.A.M., Nolan, E.A., 2001. Near-surface moisture gradients and in situ permeation tests, 'Constr. Build. Mater. 15 (2–3), 105–114. https://doi.org/10.1016/S0950-0618(00)00059-3.

Basheer, P.A.M., Nolan, É.A., McCarter, W.J., Long, A.E., 2000. Effectiveness of in situ moisture preconditioning methods for concrete. J. Mater. Civ. Eng. 12 (2), 131–138. https://doi.org/10.1061/(ASCE)0899-1561(2000)12:2(131).

P.C. Basu, P. Labbé, D.J. Naus, Nuclear power plant concrete structures, 22nd Conference on Structural Mechanics in Reactor Technology, Division VI, San Francisco, California, USA- August 18-23, 2013.

Beushausen, H., Torrent, R., Alexander, M.G., 2019. Performance-based approaches for concrete durability: state of the art and future research needs. Cem. Concr. Res. 119, 11–20. https://doi.org/10.1016/j.cemconres.2019.01.003.

Brandt, A.M., 2013. Application of concrete as a material for anti-radiation shielding – a review. Cement, Wapno, Beton, XVIII/LXXX 2, 115–132.

Bruck, P.M., Esselman, T.C., Elaidi, B.M., Wall, J.J., Wong, E.L., 2019. Structural assessment of radiation damage in light water power reactor concrete biological shield walls. Nucl. Eng. Des. 350, 9–20. https://doi.org/10.1016/j.nucengdes.2019.04.027.

Cagnon, H., Verdier, J., Nehme, A., Multon, S., 2024. Enhancing permeability measurements: bridging the gap between pressure and vacuum techniques for steady and transient states. J. Build. Eng. 94. https://doi.org/10.1016/j.jobe.2024.109933.

Castro, J., Bentz, D., Weiss, J., 2011. Effect of sample conditioning on the water absorption of concrete. Cem. Concr. Compos. 33 (8), 805–813. https://doi.org/10.1016/j.cemconcomp.2011.05.007.

Chen, W., Li, K., Wu, M.M., Liu, D.D., Wang, P., Liang, Y., 2023. Influence of pore structure characteristics on the gas permeability of concrete. J. Build. Eng. 79, 107852. https://doi.org/10.1016/j.jobe.2023.107852.

Chen, Q., Zhang, J., Wang, Z., Zhao, T., Wang, Z., 2024. A review of the interfacial transition zones in concrete: identification, physical characteristics, and mechanical properties. Eng. Fract. Mech. 300, 109979. https://doi.org/10.1016/j.engfracmech.2024.109979.

Choinska, M., Khelidj, A., Chatzigeorgiou, G., Pijaudier-Cabot, G., 2007. Effects and interactions of temperature and stress-level related damage on permeability of concrete. Cem. Concr. Res. 37 (1), 79–88. https://doi.org/10.1016/j.cemconres.2006.09.015.

D. Whiting, P.D. Cady, P. D., Condition Evaluation of Concrete Bridges Relative to Reinforcement Corrosion Volume 7: Method for Field Measurement of Concrete Permeability. Strategic Highway Research Program., in. Washington, DC, 1992.

Dąbrowski, M., Jóźwiak-Niedźwiedzka, D., Bogusz, K., Glinicki, M.A., 2022. Influence of serpentinite aggregate on the microstructure and durability of radiation shielding concrete, 127536–1 Constr. Build. Mater. 337. https://doi.org/10.1016/j.conbuildmat.2022.127536.

Das, B.B., Kondraivendhan, B., 2012. Implication of pore size distribution parameters on compressive strength, permeability and hydraulic diffusivity of concrete. Constr. Build. Mater. 28 (1), 382–386. https://doi.org/10.1016/j.conbuildmat.2011.08.055.

Domanski, S., Gryzinski, M.A., Maciak, M., Murawski, L., Tulik, P., Tyminska, K., 2016. Experimental investigation on radiation shielding of high-performance concrete for nuclear and radiotherapy facilities. Pol. J. Med. Phys. Eng. 22 (2), 41–47. https://doi.org/10.1515/pjmpe-2016-0008.

Elshazli, M.T., Ibrahim, A., Eidelpes, E., Ilevbare, G.O., 2023. Degradation mechanisms in overpack concrete of spent nuclear fuel dry storage systems: a review. Nucl. Eng. Des. 414, 112632. https://doi.org/10.1016/j.nucengdes.2023.112632.

EN 61331-1:2014, Protective devices against diagnostic medical X-radiation – Part 1: Determination of attenuation properties of materials, Edition 2.0, 2014-05.

Esen, Y., Doğan, Z.M., 2017. Evaluation of physical and mechanical characteristics of siderite concrete to be used as heavy-weight concrete. Cem. Concr. Compos. 82, 117–127. https://doi.org/10.1016/j.cemconcomp.2017.05.009.

Fabien, A., Choinska, M., Bonnet, S., Pertue, A., Khelidj, A., 2021. Aggregate size effects on the mechanical behaviour and on the gas permeability at damaged state of cement-based materials with and without slag. Eur. J. Environ. Civ. En. 26 (12), 5674–5695. https://doi.org/10.1080/19648189.2021.1915881.

K.G. Field, I. Remec, Y Le Pape, Radiation effects in concrete for nuclear power plants - Part I: quantification of radiation exposure and radiation effects, Nucl. Eng. Des. 282 (2015) 126e143, doi: 10.1016/j.nucengdes.2014.10.003.

G. ALMisned, D.S. Baykal, W. Elshami, G. Susoy, G., Kilic, H.O. Tekin, A comparative analysis of shielding effectiveness in glass and concrete containers, Open Physics, 22 (1) (2024) 20240019. doi: 10.1515/phys-2024-0019.

G. ALMisned, G. Susoy, D.S. Baykal, H.O. Tekin, A comparative investigation on mechanical, gamma-ray and neutron shielding properties of some iron and boron containing concretes samples for nuclear safety applications, Radiat. Phys. Chem, 223 (2024) 111987, doi: 10.1016/j.radphyschem.2024.111987.

Golnik, N., Gryziński, M.A., Kowalska, M., Meronka, K., Tulik, P., 2014. Characterisation of radiation field for irradiation of biological samples at nuclear reactor-comparison of twin detector and recombination method. Radiat. Prot. Dosimetry. 161 (1–4), 196–200. https://doi.org/10.1093/rpd/nct341.

Hager, I., Tracz, T., Choińska, M., Mróz, K., 2019. Effect of cement type on the mechanical behavior and permeability of concrete subjected to high temperatures. Materials 12, 3021. https://doi.org/10.3390/ma12183021.

N. W. Hayes, F. Benboudjema, Y. Le Pape, Z. John Ma, Alkali-silica reaction expansion model for confined concrete with stress-dependency and casting direction anisotropy, Cem. Concr. Res. 173 (2023) 107260, doi: 10.1016/j.cemconres.2023.107260.

He, J., Lei, D., Xu, W., 2020. In-situ measurement of nominal compressive elastic modulus of interfacial transition zone in concrete by SEM-DIC coupled method. Cem. Concr. Compos. 114, 103779. https://doi.org/10.1016/j.cemconcomp.2020.103779.

Horszczaruk, E., Brzozowski, P., 2019. Investigation of gamma ray shielding efficiency and physicomechanical performances of heavyweight concrete subjected to high temperature. Constr. Build. Mater. 195, 574–582. https://doi.org/10.1016/j.conbuildmat.2018.09.113.

Horszczaruk, E., Sikora, P., Zaporowski, P., 2015. Mechanical properties of shielding concrete with magnetite aggregate subjected to high temperature. Procedia Engineering 108, 39–46.

Huda, W., Slone, R.M., 2003. Review of radiologic physics, 2nd ed. Lippincott Williams & Wilkins, Philadelphia, p. 267.

Ihsani, R.N., Gareso, P.L., Tahir, D., 2024. An overview of gamma radiation shielding: enhancements through polymer-lead (Pb) composite materials. Radiat. Phys. Chem. 218, 111619. https://doi.org/10.1016/j.radphyschem.2024.111619.

Isfahani, H.S., Abtahi, S.M., Roshanzamir, M.A., Shirani, A., Hejazi, S.M., 2019. Investigation on gamma-ray shielding and permeability of clay-steel slag mixture. Bull Eng Geol Environ 78, 4589–4598. https://doi.org/10.1007/s10064-018-1391-6.

J. Tcherner, T. Aziz, Effects of AAR on seismic assessment of nuclear power plants for life extensions, in: Proceedings of the 20th International Conference on Structural Mechanics in Reactor Technology, SMIRT 20, Espoo, Finland, in: SMIRT20-Division 7 Paper 1789., 2009.

R. Jaya, B. Bakar, M. Johari, M. Ibrahim, M. Strength and permeability properties of concrete containing rice husk ash with different grinding time, Open Engineering, 1 (1) (2011) 103-112. doi: 10.2478/s13531-010-0003-4.

Jóźwiak-Niedźwiedzka, D., Dąbrowski, M., Brandt, A.M., Burakowska, A., Baran, T., 2018. The results of the concrete shield of the EWA nuclear reactor. Cement Wapno Beton 23 (3), 226–238.

Jóźwiak-Niedźwiedzka, D., Glinicki, M.A., Gibas, K., Baran, T., 2018. Alkali-silica reactivity of high-density aggregates for radiation shielding concrete. Materials 11, 2284. https://doi.org/10.3390/ma11112284.

Jóźwiak-Niedźwiedzka, D., Dąbrowski, M., Dziedzic, K., Jarząbek, D., Antolik, A., Denis, P., Glinicki, M.A., 2022. Effect of gamma irradiation on the mechanical properties of carbonation reaction products in mortar. Mater Struct 55, 164. https://doi.org/10.1617/s11527-022-02003-w.

Jóźwiak-Niedźwiedzka, D., Lessing, P.A., 2019. 9 - High-density and radiation shielding concrete, Editor(s): Sidney Mindess. In: Woodhead Publishing Series in Civil and Structural Engineering, Developments in the Formulation and Reinforcement of Concrete (second Edition), 193–228. Woodhead Publishing. https://doi.org/10.1016/B978-0-08-102616-8.00009-5.

M. Jung, Y. Soon Lee, S.G. Hong, J. Moon, Carbon nanotubes (CNTs) in ultra-high-performance concrete (UHPC): dispersion, mechanical properties, and electromagnetic interference (EMI) shielding effectiveness (SE), Cement Concr. Res. 131 (2020) 106017, doi: 10.1016/j.cemconres.2020.106017.

K. William, Y. Xi, D. Naus, A Review of the effects of radiation on microstructure and properties of concretes used in nuclear power plants, NUREG/CR-7171, ORNL/TM-2013/263, Division of Engineering Office of Nuclear Regulatory Research, U.S. Nuclear Regulatory Commission, Washington, DC 20555-0001, pp. 131.

Kanagaraj, B., Anand, N., Andrushia, A.D., Naser, M.Z., 2023. Recent developments of radiation shielding concrete in nuclear and radioactive waste storage facilities – a state of the art review. Constr. Build. Mater. 404, 133260. https://doi.org/10.1016/j.conbuildmat.2023.133260.

Khalaf, M.A., Ban, C.C., Ramli, M., Ahmed, N.M., Sern, L.J., Khaleel, H.A., 2020. Physicomechanical and gamma-ray shielding properties of high-strength heavyweight concrete containing steel furnace slag aggregate. J. Build. Eng. 30, 101306. https://doi.org/10.1016/j.jobe.2020.101306.

Kharita, M.H., Yousef, S., AlNassar, M., 2011. Review on the addition of boron compounds to radiation shielding concrete. Prog. Nuclear Energy. 53 (2), 207–211. https://doi.org/10.1016/j.pnucene.2010.09.012.

Khmurovska, Y., Štemberk, P., Fekete, T., Eurajoki, T., 2019. Numerical analysis of VVER-440/213 concrete biological shield under normal operation. Nucl. Eng. Des. 350, 58–66. https://doi.org/10.1016/j.nucengdes.2019.05.004.

L. J. Klinkenberg, The permeability of porous media to liquids and gases. API Drilling and Production Practice, New York, API-41-200 (1941) 200–213.

Kubissa, W., Glinicki, M.A., 2017. Influence of internal relative humidity and mix design of radiation shielding concrete on air permeability index. Constr. Build. Mater. 147, 352–361. https://doi.org/10.1016/j.conbuildmat.2017.04.177.

Kubissa, W., Glinicki, M.A., Dąbrowski, M., 2018. Permeability testing of radiation shielding concrete manufactured at industrial scale. Mater. Struct. 51 (83), 1–15. https://doi.org/10.1617/s11527-018-1213-0.

Kuć, M., 2023. Fast method of determining the ambient dose equivalent at a depth of 10 mm of gamma-neutron fields based on recombination methods. Radiat. Prot. Dosimetry. 11 (199), 1872–1876. https://doi.org/10.1093/rpd/ncad016.

Kuć, M., Maciak, M., Tulik, P., 2024. A sub-picoampere measurement algorithm for use in dosimetry of time-varying radiation fields. Sensors 24 (6), 2012. https://doi.org/10.3390/s24062012.

Lardhi, M., Mukhtar, F., 2023. Radiation shielding performance of seawater-mixed concrete incorporating recycled coarse aggregate and steel slag. J. Radiat. Res. Appl. Sci. 16, 100528. https://doi.org/10.1016/j.jrras.2023.100528.

Lehner, P., Gołaszewski, J., 2021. Relationship of different properties from non-destructive testing of heavy concrete from magnetite and serpentinite. Materials 14, 4288. https://doi.org/10.3390/ma14154288.

Lotti, P., Comboni, D., Gigli, L., Carlucci, L., Mossini, E., Macerata, E., Mariani, Ma., Gatta, G.D., 2019. Thermal stability and high-temperature behavior of the natural borate colemanite: an aggregate in radiation-shielding concretes. Constr. Build. Mater. 679–686. https://doi.org/10.1016/j.conbuildmat.2019.01.123.

Madej, D., Cherkes, P., Silarski, M., 2024. Effect of temperature on gamma radiation shielding capabilities of bauxite-based refractory concrete. Cem. Concr. Compos. 152, 105608. https://doi.org/10.1016/j.cemconcomp.2024.105608.

Maruyama, I., Kontani, O., Sawada, S., Sato, O., Igarashi, G., Takizawa, M., 2013. Evaluation of irradiation effects on concrete structure – background and preparation of neutron irradiation test. In: Proceedings of the ASME 2013 Power Conference POWER2013.

Maruyama, I., Kontani, O., Takizawa, M., Sawada, S., Ishikawao, S., Yasukouchi, J., Sato, O., Etoh, J., Igari, T., 2017. Development of soundness assessment procedure for concrete members affected by neutron and gamma-ray irradiation. J. Adv. Concr. Technol. 15 (9), 440–523. https://doi.org/10.3151/jact.15.440.

Masoud, M.A., El-Khayatt, A.M., Mahmoud, K.A., Rashad, A.M., Shahien, M.G., Bakhit, B. R., Zayed, A.M., 2023. Valorization of hazardous chrysotile by H_3BO_3 incorporation to produce an innovative eco-friendly radiation shielding concrete: implications on physico-mechanical, hydration, microstructural, and shielding properties. Cem. Concr. Compos. 141, 105120. https://doi.org/10.1016/j.cemconcomp.2023.105120.

R. Meiswinkel, J. Meyer, J. Schnell, Design and construction of nuclear power plants, Beton-Kalender Series (2013) Ernst & Sohn, pp. 150.

Miah, M.J., Kallel, H., Carré, H., Pimienta, P., La Borderie, C., 2019. The effect of compressive loading on the residual gas permeability of concrete. Constr. Build. Mater. 217, 12–19. https://doi.org/10.1016/j.conbuildmat.2019.05.057.

V. Miana Radja, F. Haryanti Viorekta, I. Wahyuning Tyas, Relationship between relative density and land permeability in ende flores area, Int. J. Adv. Eng. Manag. 3(7) (2021) 3032-3037, doi: 10.35629/5252-030730323037.

Mostofinejad, D., Reisi, M., Shirani, A., 2012. Mix design effective parameters on γ-ray attenuation coefficient and strength of normal and heavyweight concrete. Constr. Build. Mater. 28 (1), 224–229. https://doi.org/10.1016/j.conbuildmat.2011.08.043.

Němeček, J., Trávníček, P., Keppert, M., Halodová, P., Rosnecký, V., Němeček, J., 2023. Nanomechanical analysis of Gamma-irradiated cement paste exposed to different humidities. Constr. Build. Mater. 393, 131969. https://doi.org/10.1016/j.conbuildmat.2023.131969.

Oto, B., Yıldız, N., Korkut, T., Kavaz, E., 2015. Neutron shielding qualities and gamma ray buildup factors of concretes containing limonite ore. Nucl. Eng. Des. 293, 166–175. https://doi.org/10.1016/j.nucengdes.2015.07.060.

Ouda, A.S., 2015. Development of high-performance heavy density concrete using different aggregates for gamma-ray shielding. Prog. Nuclear Energy 79, 48–55. https://doi.org/10.1016/j.pnucene.2014.11.009.

A. Pazirandeh, A. Torkamani, A. Taheri, Design and simulation of a neutron source based on an electron linear accelerator for BNCT of skin melanoma, Appl. Radiat. Isot. 69 (5) (2011) 749e755, doi: 10.1016/j.apradiso.2011.01.035.

Pei, Y., Li, S., Agostini, F., Skoczylas, F., Masson, B., 2019. Sealing of concrete confining structures of French nuclear reactors. Eng. Struct. 197, 109283. https://doi.org/10.1016/j.engstruct.2019.109283.

PN-B-06265:2018 Concrete. Requirements, properties, production and compliance – national supplement to PN-EN 206, Polish Committee for Standardization, Warsaw, 2018.

PN-B-06714-40: 1978 Mineral aggregates. Testing. Determination of crushing strength, Polish Committee for Standardization, Warsaw, 1978.

PN-EN 12390-7:2019-08, Testing hardened concrete - Part 7: Density of hardened concrete, PKN/KT 274, 2020-07-20, pp. 14.

PN-EN 12390–3:2019-07, Testing hardened concrete - Part 3: Compressive strength of test specimens, PKN/KT 274, 2020-07-20, pp. 22.

PN-EN 1367-1:2007 Tests for thermal and weathering properties of aggregates. Determination of resistance to freezing and thawing, Polish Committee for Standardization, Warsaw, 2007.

PN-EN 1097-6:2013 Tests for mechanical and physical properties of aggregates. Determination of particle density and water absorption, Polish Committee for Standardization, Warsaw, 2013.

B. Pomaro, A review on radiation damage in concrete for nuclear facilities: from experiments to modelling, Model. Simul. Eng. (2016) Article ID 4165746, pp.10, doi: 10.1155/2016/4165746.

R. Torrent, G. Frenzer, G., A method for rapid determination of the coefficient of permeability of the “covercrete”, in International Symposium Non-Destructive Testing in Civil Engineering (1995) 985–992.

Reches, Y., 2019. A multi-scale review of the effects of gamma radiation on concrete. Results in Materials 2, 100039. https://doi.org/10.1016/j.rinma.2019.100039.

S. M. Rasoul Abdar Esfahani, S.A. Zareei, M. Madhkhan, F. Ameri, J. Rashidiani, R.A. Taheri, Mechanical and gamma-ray shielding properties and environmental benefits of concrete incorporating GGBFS and copper slag, J. Build. Eng., 33 (2021) 101615, doi: 10.1016/j.jobe.2020.101615.

Saafan, M.A., Etman, Z.A., Jaballah, A.S., Abdelati, M.A., 2023. Strength and nuclear shielding performance of heavyweight concrete experimental and theoretical analysis using WinXCom program. Prog. Nuclear Energy 160, 104688. https://doi.org/10.1016/j.pnucene.2023.104688.

Saklani, N., Banwat, G., Spencer, B., Rajan, S., Sant, G., Neithalath, N., 2021. Damage development in neutron-irradiated concrete in a test reactor: hygro-thermal and mechanical simulations. Cement Concr. Res. 142, 106349. https://doi.org/10.1016/j.cemconres.2020.106349.

Sayyadi, A., Mohammadi, Y., Adlparvar, M.R., 2022. Effect of serpentine aggregates on the shielding, mechanical, and durability properties of heavyweight concrete. Int. J. Eng. Trans. b: Appl 35 (11), 2256–2264. https://doi.org/10.5829/ije.2022.35.11b.21.

Shams, T., Eftekhar, M., Shirani, A., 2018. Investigation of gamma radiation attenuation in heavy concrete shields containing hematite and barite aggregates in multi-layered and mixed forms. Constr. Build. Mater 182, 35–42. https://doi.org/10.1016/j.conbuildmat.2018.06.032.

Shi, J., Liu, B., Wu, X., Qin, J., Jiang, J., He, Z., 2020. Evolution of mechanical properties and permeability of concrete during steam curing process. J. Build. Eng. 32, 101796. https://doi.org/10.1016/j.jobe.2020.101796.

Sogbossi, H., Verdier, J., Multon, S., 2019. New approach for the measurement of gas permeability and porosity accessible to gas in vacuum and under pressure. Cem. Concr. Compos. 103, 59–70. https://doi.org/10.1016/j.cemconcomp.2019.04.032.

Sommers, F., 1969. Gamma radiation damage of structural concrete immersed in water. Health Physics 16 (4), 503–508.

Soo, P., Milian, L.M., 2001. The effect of gamma radiation on the strength of Portland cement mortars. J. Mater. Sci. Lett. 20 (14), 1345–1348.

Tekin, H.O., Sayyed, M.I., Issa, S.A.M., 2018. Gamma radiation shielding properties of the hematite-serpentine concrete blended with WO_3 and Bi_2O_3 micro and nano particles using MCNPX code. Radiat. Phys. Chem. 95–100. https://doi.org/10.1016/j.radphyschem.2018.05.002.

Tekin, H.O., Kaçal, M.R., Issa, S.A.M., Polat, H., Susoy, G., Akman, F., Kilicoglu, O., Gillette, V.H., 2020. Sodium dodecatungstophosphate hydrate-filled polymer composites for nuclear radiation shielding. Mater. Chem. Phys. 123667. https://doi.org/10.1016/j.matchemphys.2020.123667.

Tracz, T., 2016. Open porosity of cement pastes and their gas permeability. Bull. Pol. Acad. Sci. 64 (4), 775–783. https://doi.org/10.1515/bpasts-2016-0086.

Wang, J.-L., et al., 2023. Heavy concrete shielding properties for carbon therapy. Nucl. Eng. Technol. 55 (6), 2335–2347. https://doi.org/10.1016/j.net.2023.03.003.

XP P 18-463, Concrete - Testing gas permeability on hardened concrete, 2011.

Yadollahi, A., Nazemi, E., Zolfaghari, A., Ajorloo, A.M., 2016. Optimization of thermal neutron shield concrete mixture using artificial neural network. Nucl. Eng. Des. 305, 146–155. https://doi.org/10.1016/j.nucengdes.2016.05.012.

Yang, S., Zhongzi, X., Mingshu, T., 1998. Improving the structure of the interfacial zone and its influence on the long-term behavior of mortars. Mat. Struct. 31, 230–234. https://doi.org/10.1007/BF02480420.

Y-Ch. Kan, K.-Ch. Pei, C.-L. Chang, Strength and fracture toughness of heavy concrete with various iron aggregate inclusions, Nucl. Eng. Des. 228, 1–3 (2004) 119-127, doi: 10.1016/j.nucengdes.2003.06.008.

H.M.H. Zakaly, G. ALMisned, S.A.M. Issa, Towards a better understanding of filler size on radiation shielding enhancement: impact of micro- and nano-WO_3/PbO particle reinforcement on ILC concrete. J Aust Ceram Soc 59 (2023) 127–135. doi: 10.1007/s41779-022-00818-y.

A.M. Zayed, A.M. El-Khayatt, Petros Petrounias, M.G. Shahien, K.A. Mahmoud, Alaa M. Rashad, Ahmed H. Ragab, Abeer A. Hassan, Bottros R. Bakhit, M.A. Masoud, From discarded waste to valuable products: Barite combination with chrysotile mine waste to produce radiation-shielding concrete, Constr. Build. Mater. 417 (2024) 135334, doi: 10.1016/j.conbuildmat.2024.135334.

Zayed, A.M., Masoud, M.A., Shahien, M.G., Gökçe, H.S., Sakr, K., Kansouh, W.A., El-Khayatt, A.M., 2021. Physical, mechanical, and radiation attenuation properties of

serpentine concrete containing boric acid. Constr. Build. Mater. 272, 121641. https://doi.org/10.1016/j.conbuildmat.2020.121641.
Zhang, J., Bian, F., Zhang, Y., Fang, Z., Fu, C., Guo, J., 2018. Effect of pore structures on gas permeability and chloride diffusivity of concrete. Constr. Build. Mater. 163, 402–413. https://doi.org/10.1016/j.conbuildmat.2017.12.111.
Zhang, Y., Fang, L., Wu, S., Du, S., Zhang, J., 2022. Time dependency and similarity of gas permeability of concrete in simulated environment. J. Build. Eng. 51, 104253. https://doi.org/10.1016/j.jobe.2022.104253.
Zhou, Y., Chen, X., Zhan, Y., Sun, F., Zhang, J., He, W., 2023. Research on the shielding performance of concrete in a ^{60}Co irradiation environment. Nucl. Eng. Des. 413, 112575. https://doi.org/10.1016/j.nucengdes.2023.112575.
Zou, C., Zheng, S., Chen, Z., Long, G., Xiao, J., 2024. Effects of aggregate preheating and polymer fibers on the mechanical, thermal and radiation shielding properties of barite concrete. Constr. Build. Mater. 442, 137533. https://doi.org/10.1016/j.conbuildmat.2024.137533.